Chinese Physical Society | IOP Publishing
CPB
Chinese Physics B
http://cpb.iphy.ac.cn https://iopscience.iop.org/journal/1674-1056

Tuning charge and orbital ordering in $DyNiO_3$ by biaxial strain

Litong Jiang(姜丽桐), Kuijuan Jin(金奎娟), Wenning Ren(任文宁), and Guozhen Yang(杨国桢)

Citation: Chin. Phys. B, 2021, 30 (**11**): 117106. DOI: 10.1088/1674-1056/abfbcf
Journal homepage: http://cpb.iphy.ac.cn; http://iopscience.iop.org/cpb

Tuning charge and orbital ordering in $DyNiO_3$ by biaxial strain*

Litong Jiang(姜丽桐)[1,2], Kuijuan Jin(金奎娟)[1,2,3,†], Wenning Ren(任文宁)[1,2], and Guozhen Yang(杨国桢)[1,2,3]

[1] *Beijing National Laboratory for Condensed Matter Physics, Institute of Physics, Chinese Academy of Sciences, Beijing* 100190, *China*

[2] *School of Physical Sciences, University of Chinese Academy of Sciences, Beijing* 100049, *China*

[3] *Songshan Lake Materials Laboratory, Dongguan* 523808, *China*

(Received 31 March 2021; revised manuscript received 21 April 2021; accepted manuscript online 27 April 2021)

The first-principles calculations were used to explore the tunable electronic structure in $DyNiO_3$ (DNO) under the effects of the biaxial compressive and tensile strains. We explored how the biaxial strain tunes the orbital hybridization and influences the charge and orbital ordering states. We found that breathing mode and Jahn–Teller distortion play a primary role in charge ordering state and orbital ordering state, respectively. Additionally, the calculated results revealed that the biaxial strain has the ability to manipulate the phase competition between the two states. A phase transition point has been found under tensile train. If the biaxial train is larger than the point, the system favors orbital ordering state. If the strain is smaller than the point, the system is in charge ordering state favorably.

Keywords: charge ordering, orbital ordering, Jahn–Teller distortion, biaxial strain

PACS: 71.70.Fk, 31.15.–p, 31.15.A–, 31.15.ae **DOI:** 10.1088/1674-1056/abfbcf

1. Introduction

The rare-earth nickelates, RNiO$_3$ (RNO, R strands for La or Ce, Pr, …, Lu of the rare-earth series), have been studied for decades, because of a large variety of the possible physical properties.[1–4] Actually, this material is a type of ABO_3 perovskites. The R element locates on the A site and the Ni locates on the B site. An ideal RNO perovskite, which has six equal Ni–O bond lengths in its NiO_6 octahedra, is in $Pm\bar{3}m$ phase.[4] RNO has a sharp metal–insulator transition, except $R = $ La. This transition temperature ($T_{\rm MI}$) increases as the R cation decreases.[5,6]

The structural changes of $DyNiO_3$ (DNO), one in the family of RNiO$_3$ perovskite rare-earth nickelates, leading to the metal–insulator transition ($T_{\rm MI} = 564$ K), have been explored via experiments.[7] This sharp transition is accompanied by a structural phase transition. Below $T_{\rm MI}$, namely, in the insulating or semi-conducting regime, DNO favors monoclinic with $P2_1/n$ space group. The charge disproportionation breaks the equivalent NiO_6 octahedra into two nonequivalent ones: a type of NiO_6 octahedra with longer bonds (Ni_L) and the other type of octahedra with shorter bonds (Ni_S), which results from charge ordering.[3,6,8] Above $T_{\rm MI}$, DNO becomes orthorhombic with *Pbnm* space group with orbital ordering states. Experiments show that $T_{\rm MI}$ is related to the strength of the orthorhombic distortion.[9]

For the basic electronic configuration, normally, the chemical valence of Ni ions is +3, with the low-spin d^7 electronic configuration, where t_{2g} orbitals are fully occupied and only one electron left in the two e_g orbitals, if we assume that the NiO_6 octahedra are perfect.[10] Those two e_g orbitals are supposed be equally occupied without the crystal field induced by the orthorhombic distortion. In reality, RNO can be illustrated by a charge transfer energy Δ, because of the hopping between O 2p and the Ni d orbitals. The ligand hole in the oxygen 2p bands is denoted by L.[11] So the ground state in RNO should be illustrated as a mixture of d^7 and d^8L. This could explain that, in recent years, the configuration of $P2_1/n$ is more commonly used as $2\times\left(d^7\right) \rightarrow d^8 + d^8L^2$ rather than $2\times\left(d^7\right) \rightarrow d^8 + d^6$ at Ni sites.[12] In *Pbnm* phase, the Ni ions are more commonly used as $3d^7$ or $3d^8$L.[13,14] Regularly, the nominal d^7 configuration is stable under a Jahn–Teller distortion, which is assumed to follow an electronic driving force,[8] aiming for removing the degeneracy of the e_g orbitals.[15] The electron occupation of the 3d orbitals leads to rich physics, via the hybridization of Ni and O, which can be manipulated by structural changes.

The substrate fixes the in-plane lattice constants of epitaxial growth films with distortions, rotations, octahedral tilts, and lattice symmetry, so that the thin films behave differently from their bulk counterpart.[16,17] The crystal structures of nickelates are capable of being tuned by producing epitaxial films on various substrates, which has been reported in several materials of RNO family under the in-plane biaxial strain.[2,17–20] Because of the in-plane mismatch, the out-of plane lattice parameter of the film will be stretched or compressed. Consequently, the oxygen octahedra obtain the staggered Jahn–Teller distortion under the tensile strain or the charge disproportion under sufficient compressive strain.[10]

*Project supported by the National Key Basic Research Program of China (Grant No. 2019YFA0308500), the National Natural Science Foundation of China (Grant No. 11721404), and the Strategic Priority Research Program (B) of the Chinese Academy of Sciences (Grant No. XDB33030200).

†Corresponding author. E-mail: kjjin@iphy.ac.cn

For *R*NO, epitaxial strain is a widely investigated method to manipulate functional properties.[17–22] Mikheev *et al.* reported that $NdNiO_3$ thin films are capable of being manipulated between the paramagnetic metallic state and the antiferromagnetic insulating state by applying epitaxial strain and changing thickness.[23] So many research works tried strain engineering to obtain charge or orbital ordering of e_g orbitals for other common nickelates in *R*NO series.[24–26] He *et al.* explored the $LuNiO_3$ under biaxial strain in Ref. [24], which revealed that with sufficient applied strain (around 4%) the system undergoes a first-order transition. Zhang *et al.* suggested that the metal–insulating transition temperature is relevant to symmetry. Since T_{MI} is suppressed in $NdNiO_3/YAlO_3$ by tuning the distortion of the epitaxial films.[25] Varignon *et al.* focused on $PrNiO_3$ and $NdNiO_3$ in Ref. [26], which reported that the first order phase transition can be tuned by strain. But no study about the strain effect in DNO has been reported yet. In this paper, by carrying out density functional theory (DFT) calculation, we present that a sufficient applied tensile strain forces the system into a non-charge-ordered state. Additionally, the staggered Jahn–Teller distortion can be characterized by this tensile strain. We also show how the in-plane biaxial compressive and tensile strains modify the electronic configuration. This work provides some theoretical results for further experiments about growing DNO thin films for manipulating its electronic structures.

2. Method

Our DFT calculations were conducted by general-gradient approximation (GGA) with the Perdew–Burke–Ernzerhof revised for solids (PBEsol)[27] and projector augmented wave (PAW) method[28] as implemented in the Vienna *ab initio* simulation package (VASP).[29] For the relaxation part, the $6\times6\times2$ centered *k*-point meshes were used. For magnetism, we considered four 20-atom-structure antiferromagnetic configurations: A-type antiferromagnetic (A-AFM), C-type antiferromagnetic (C-AFM), G-type antiferromagnetic (G-AFM), and ferromagnetic (FM) ones. Here, a Hubbard U correction[30] with $U_{Ni} = 2$ eV ($J = 0$ eV) was added to improve the description of the electronic structure of Ni (transition metal). Previous works showed that a small U was used normally for describing nickelates accurately.[31,32] Some articles reported that $U(\mathrm{Ni}) = 0$–6 eV does not impact the crystal geometry very much.[21,26,33] Some articles showed different values of U have negligible effects on the crystal structure, but open the band gap with larger U.[30] Here, we also used other U values (i.e., 1 eV, 3 eV, 4 eV, 5 eV, and 6 eV). The PAW potentials were Ni ($3p^6 3d^8 4s^2$), Dy ($6s^2 6p$), and O ($2s^2 2p^4$). The energy cutoff was 540 eV. The bond lengths and octehedra volumes were read via VESTA.[34]

3. Results

We calculated the ground state structure of DNO, which is in $P2_1/n$ phase. Figure 1 shows the crystal structure of the system which is obtained by DFT $+U$ calculations. The lattice parameters of DNO are listed in Table 1. Our optimized parameters are very close to the experimental ones.[7,33] The in-plane pseudocubic lattice parameter $a = 3.78$ Å ($a = (\sqrt{a^2+b^2})/2$), which is half of the diagonal of the primitive cell. Because the in-plane lattice parameters of the film must fix with the lattice constants of the substrate. An in-plane lattice mismatch η is defined as $\eta = (a_{sub} - a')/a'$. Here, a' denotes the in-plane lattice constant of the DNO under biaxial strain and a_{sub} denotes the in-plane lattice constant of the substrate. All the parameters mentioned above in this paper are pseudocubic parameters.

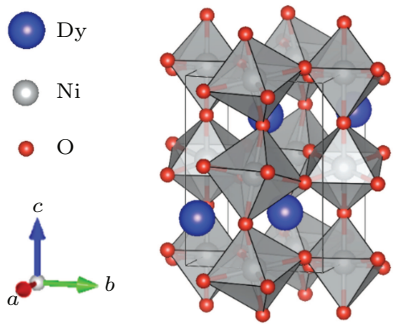

Fig. 1. The structure of the ground state of DNO in $P2_1/n$ space group. NiO_6 octahedra are illustrated by gray cubes. The navy, gray, and red spheres represent Dy, Ni, and O atoms, respectively.

Table 1. Calculated optimized and experimental lattice parameters of DNO.

Lattice parameters	Calc. (Å)	Expt.[a] (Å)
a	5.51	5.48
b	5.18	5.11
c	7.42	7.32

[a]Refs. [7,33].

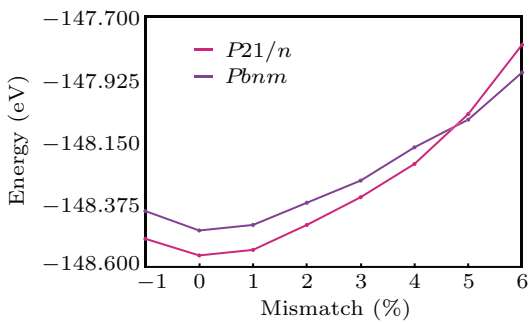

Fig. 2. Total energy versus lattice mismatch. The purple line represents *Pbnm* phase; the pink line represents $P2_1/n$ phase.

The energy of DNO with applied compressive or tensile biaxial strain is plotted in Fig. 2. A first-order phase transition from $P2_1/n$ to *Pbnm* occurs driven by the tensile strain, obviously. Since the energy of the $P2_1/n$ phase is lower than that of the *Pbnm* phase when the tensile strain is less than 4.7%, which also means the charge ordering is more stable.

The transition occurs in the *ab* plane around 4.7% mismatch, corresponding to $a_{\text{sub}} = 3.95$ Å. In contrast, the orbital ordering (*Pbnm*) phase is energetically favorable, if the mismatch under tensile strain is larger than 4.7%.

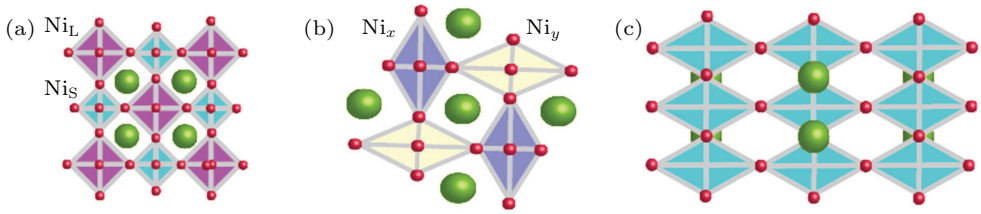

Fig. 3. The schemes of (a) breathing modes. (b) Type-d Jahn–Teller distortion and (c) type-a Jahn–Teller distortion.

Figure 3 demonstrates the diagrams of octahedra distions in breathing mode and Jahn–Teller distortions. In the breathing mode, as depicted in Fig. 3(a), the Ni$_L$ and Ni$_S$ are adjacent alternatively. A large difference between the Ni$_L$ and Ni$_S$ octahedra implies a strong breathing mode. For the Jahn–Teller distortions, there are two types, which play important roles under biaxial strains. The one, which forces the shrink of z direction of the octahedra, is named by type-a Jahn–Teller distortion in Fig. 3(c). The other one, which distorts the in-plane bonds of the octahedron, is termed as type-d Jahn–Teller distortion (see Fig. 3(b)). The Ni$_x$ is defined as its Ni–O bonds in x direction longer than that in y direction in an octahedron. Meanwhile, in the adjacent octahedron Ni$_y$, the Ni–O bonds along x direction are shorter than that along y direction.

Before exploring the distortions in DNO under biaxial strain, it is to be mentioned that, the *Pbnm* crystal structure is very close to its bulk crystal structure and is far away from the $P2_1/n$ bulk crystal structure after relaxation. Moreover, the symmetry of *Pbnm* crystal structure is lower than that of $P2_1/n$. Therefore, it is reasonable to use the *Pbnm* to denote the state without charge disproportionation, and use the $P2_1/n$ to denote the state with charge disproportionation. We use symmetrical vibration modes to illustrate the lattice distortions and phase transition in DNO under biaxial strain. The breathing mode can be characterized by Q_1 mode, as shown in Fig. 4(a). The strength of the Q_1 mode is defined as Eq. (1). The Q_1 values can represent the shrink or expansion of the NiO_6 octahedra. The difference between Q_1 values of adjacent octahedra (Ni$_S$ and Ni$_L$) is shown in Fig. 3(a). The larger difference leads to a strong breathing mode. The Jahn–Teller distortions can be specified by Q_2 and Q_3 modes (see Figs. 4(b) and 4(c)). The strengths of Q_2 and Q_3 modes are defined as Eqs. (2) and (3), respectively.[35,36] The larger Q_2 and Q_3 that we obtain in the system, the stronger the type-d and type-a Jahn–Teller distortion occur.

$$Q_1 = (L_S + L_M + L_L)/\sqrt{3}, \tag{1}$$

$$Q_2 = (L_L - L_M)/\sqrt{2}, \tag{2}$$

$$Q_3 = (2L_S - L_M - L_L)/\sqrt{6}, \tag{3}$$

where L_L, L_M, and L_S represent the long, medium, and short (z direction) Ni–O bonds, respectively.

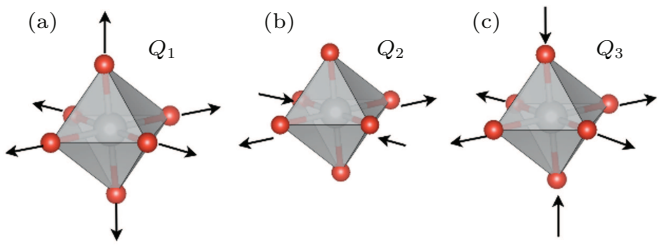

Fig. 4. (a)–(c) The Q_1, Q_2, and Q_3 modes. The arrows illustrate the displacements generated by the displacement of the oxygen atoms with respect to the regular octahedron.

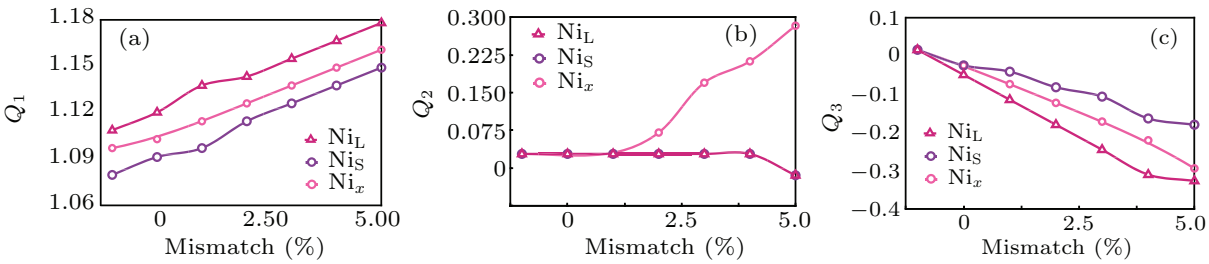

Fig. 5. (a)–(c) Calculated Q_1, Q_2, and Q_3 given by Eqs. (1), (2), and (3) versus lattice mismatch of Ni$_L$, Ni$_S$, Ni$_x$, and Ni$_y$.

Figure 5 demonstrates the changing trend of Q_1, Q_2, and Q_3 under the impact of the lattice mismatch. In Fig. 5(a), the increase in Q_1 means the expansion of the NiO_6 octahedra becomes larger with the increasing tensile strain. The difference between the values of Q_1 for Ni$_L$and Ni$_S$ in the charge ordering phase is larger than zero. This can be understood that the purple cubes are larger than the crayon ones, as shown in Fig. 3(a). As mentioned above, it means the breathing mode does exist. However, when the mismatch is larger than 4.7%, the breathing mode vanishes in the orbital ordering phase, be-

cause of the zero difference between the values of Q_1 for Ni_x and Ni_y. In Fig. 5(b), Q_2 of Ni_x is near zero under the compressive strain. With the increasing tensile strain, Q_2 rises promptly. This helps us to explain the emergency of type-d Jahn–Teller distortion in the *Pbnm* phase. In Fig. 5(c), Q_3 for both states shrinks, when the lattice mismatch gets larger. This can be accepted that the lattice constant c is compressed when the film grows on a substrate with large lattice. So, it concludes that the tensile strain strengthens the type-a Jahn–Teller distortion efficiently.

Then, we focus on the electronic structure of DNO. The O 2p bands hybridize with the e_g orbitals of Ni_S, because the stronger Coulomb repulsion is induced by the shorter distance between the Ni and O. For the charge ordering phase, the splitting energy of e_g/t_{2g} in Ni_S is larger than that of Ni_L, resulting in the energy difference of e_g in the two neighboring Ni ions and a charge ordering. So, Ni–O octahedron being expanded can localize the Ni_L e_g states, which further results in a relatively larger magnetic moment. The Ni_L obtains 1.2 μ_B, according to our calculations. These results are in agreement with that the charge ordering is more likely to be $2\times 3d^8L \rightarrow 3d^8 + 3d^8L^2$.[11,13,14,32] In the orbital ordering state, one of the e_g states is occupied alternately. A longer bond of Ni–O is less capable of attracting charge than a shorter one, which is formed by the hybridization between O 2p and Ni 3d. This is consistent with the result that the real charge value is more than 7 by our calculations. For the Ni_x in orbital ordering, the tensile strain strengthens the JT distortion, leading to a splitting of e_g levels, which enhances the orbital ordering.

We then represent the orbital-resolved electronic density of states (DOS) of Ni_S, Ni_L, and Ni_x (see Fig. 6). The different DOS between Ni_S and Ni_L sites also interprets their different electronic states. The calculated orbital-resolved density of states of Ni_S and Ni_L in $P2_1/n$ phase is presented in Fig. 6, where five d orbitals are divided by Jahn–Teller distortion into distinct orbitals e_g and t_{2g}, respectively. These results indicate that e_g and t_{2g} orbitals of the Ni atoms split into a high and a low energy regions. In Fig. 6(a), the major spins of the Ni_L orbitals are mostly occupied. In Fig. 6(c), the minor spins of the e_g orbitals are basically unoccupied. In contrast, Ni_S e_g orbitals (major spin) are occupied partly, with the t_{2g} orbitals are fully occupied, as shown in Figs. 6(b) and 6(d). From the DOS configuration, it is shown that the DOS splitting in the 3d shell of Ni_L is more strong than that of Ni_S.

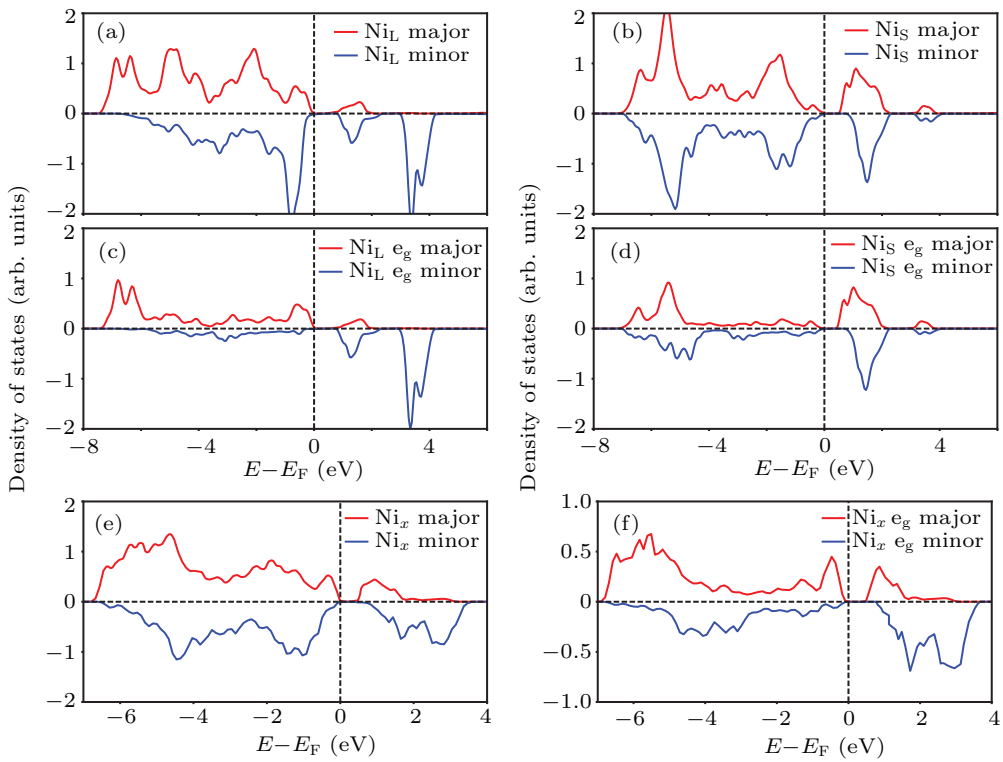

Fig. 6. The local and projected density of states of (a)–(d) the Ni_L and Ni_S in $P2_1/n$ structure (charge ordering state) under compressive strain (mismatch = −1%); (e), (f) Ni_x in *Pbnm* structure (orbital ordering state) under tensile strain (mismatch = 4%). The red (blue) color denotes the major spin (minor spin) states.

The electrons and bonds behaviors in DNO can be characterized by the contour maps of charge densities in (001) and (110) slices, as shown in Fig. 7. In the orbital ordering state, it is proved that the Ni_x and Ni_y octahedra are bond centered instead of charge centered (see Fig. 7(a)). Because the longer bonds between the Ni_x and O 2p are only in the x direction. Furthermore, the rotation symmetry between neighboring octahedra is consistent with the e_g alternate occupations. In Fig. 7(b), the disproportional bonds arrangement along x direction and equivalent arrangement along z direction are con-

sistent with the in-plane Jahn–Teller distortion. For the charge ordering state, the Ni_S ions have obvious Ni_S–O 2p hybridization which is consistent with the electronic configuration of Ni_S with $3d^8 + 3d^8L^2$ in both (110) and (001) slices, as shown in Figs. 7(c) and 7(d). Figures 6(e), 6(f), 7(a), and 7(b) are helpful to explain the electronic arrangement for the orbital ordering phase. Here, three almost empty e_g orbitals (blue) are above the Fermi level with only one occupied spin e_g orbital (red) left. It implies that the hybridization between Ni_x and O 2p states obtains a significant occupation.

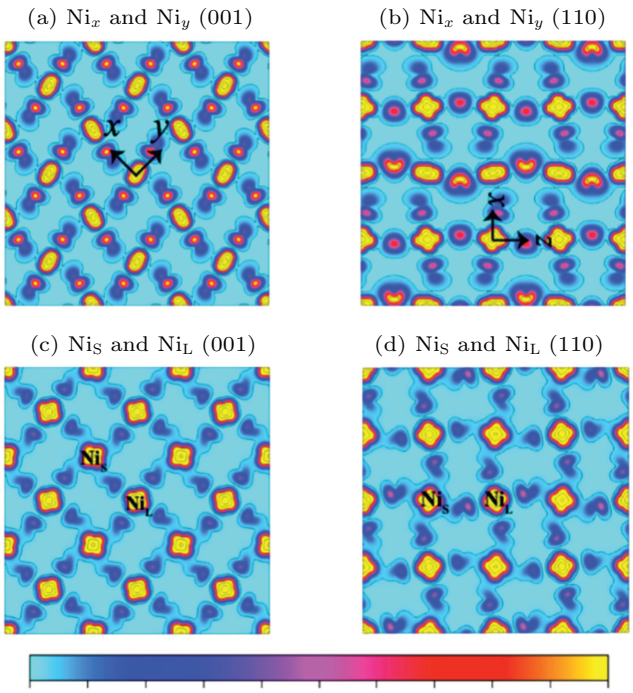

Fig. 7. The contour maps of the electron density: (a), (b) Ni_x in *Pbnm* structure (OO state) in (001) and (110) slices; (c), (d) Ni_S and Ni_L in $P2_1/n$ structure (charge ordering state) in (001) and (110) slices. The red green blue (RGB) color scale range bar is given. The RGB scale represents electron density from low (green) to high (yellow).

The band gap has been calculated to explore its change with biaxial strain in Fig. 8. The band gap shrinks gradually at the beginning with the tensile strain in charge ordering phase. But in the orbital ordering phase, it becomes larger with the tensile strain. Because the top of the valence band is composed of Ni_L bonds; the bottom of the conduction band is composed of Ni_S e_g bands. The e_g energy shift induces the band gap, which is connected with the strength of the bond disproportionation. It is capable of shifting Ni_L e_g orbitals downward and the Ni_S e_g orbitals upward. So that the breathing mode opens the gap, which can explain that change in band gap is larger with the enhanced charge ordering phase. The splitting of the e_g orbital induces the generation of the band gap, where the band gap of the orbital ordering structure increases with the tensile strain. In the orbital ordering, the e_g orbitals (major spin) are mostly unoccupied. So, the gap is enlarged by the type-d Jahn–Teller distortion. Additionally, the tensile strain in the orbital ordering phase is capable of enlarging both type-d and type-a Jahn–Teller distortions and then opens the band gap, which is in agreement with Fig. 8.

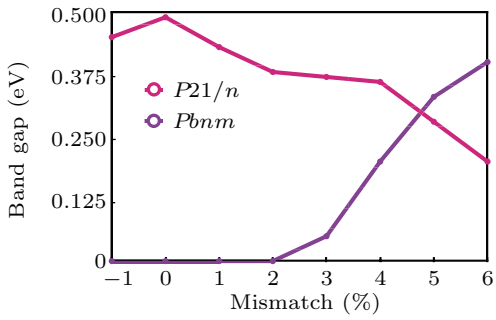

Fig. 8. Band gap of DNO versus lattice mismatch. The purple line represents *Pbnm* phase and the pink line represents $P2_1/n$ phase.

4. Conclusion and perspectives

The density functional theory has been used to analyze the effects of biaxial strain on the electronic configuration of the transition between charge ordering state and orbital ordering state in DNO. Our calculations have shown that with large enough tensile strain, the charge ordering vanishes. But the orbital ordering emerges at the lattice mismatch $\eta = 4.7\%$. This transition proves that the emergence of type-d Jahn–Teller mode is encouraged by tensile strain. The breathing mode is encouraged by compressive strain. In the charge ordering state, the breathing mode induces the difference between the neighboring NiO_6 octahedra and splitting of e_g/t_{2g}, which leads to a charge transfer between Ni_S and Ni_L. The Ni_S is with the configuration of $3d^8L^2$, because of the strong hybridization with O 2p. The Ni_L has a higher occupation of $3d^8$, since its lower e_g energy level. By applying biaxial strain from $\eta = -1\%$ to $\eta = 6\%$, the band gap becomes narrow gradually at first but becomes wide slightly in the orbital ordering state. In the same situation, type-d Jahn–Teller distortion is enhanced in orbital ordering state, but the breathing mode is shrunk in charge ordering state. Finally, we hope that these results can inspire the relative experimental research on manipulating the electronic structure in $DyNiO_3$.

References

[1] Staub U, Meijer G I, Fauth F, Allenspach R, Bednorz J G, Karpinski J, Kazakov S M, Paolasini L and d'Acapito F 2002 *Phys. Rev. Lett.* **88** 126402

[2] Fernandez-Diaz M T, Alonso J A, Martinez-Lope M J, Casais M T, Garcia-Munoz J L and Aranda M A G 2000 *Physica B* **276** 218

[3] Alonso J A, García-Muñoz J L, Fernández-Díaz M T, Aranda M A G, Martínez-Lope M J and Casais M T 1999 *Phys. Rev. Lett.* **82** 3871

[4] Mizokawa T, Khomskii D and Sawatzky G 2000 *Phys. Rev. B* **61** 11263

[5] Hwang H Y 2006 *MRS Bulletin* **31** 28

[6] Medarde M L 1997 *J. Phys.: Condens. Matter* **9** 1679

[7] Alonso J A, Martinez-Lope M J, Demazeau G, Fernandez-Diaz M T, Presniakov I A, Rusakov V S, Gubaidulina T V and Sobolev A V 2008 *Dalton Trans.* **46** 6584

[8] Catalano S, Gibert M, Bisogni V, Peil O E, He F, Sutarto R, Viret M, Zubko P, Scherwitzl R, Georges A, Sawatzky G A, Schmitt T and Triscone J M 2014 *APL Materials* **2** 116110

[9] Barman S R, Chainani A and Sarma D D 1994 *Phys. Rev. B* **49** 8475

[10] Middey S, Chakhalian J, Mahadevan P, Freeland J W, Millis A J and Sarma D D 2016 *Ann. Rev. Mater. Res.* **46** 305

[11] Bisogni V, Catalano S, Green R J, Gibert M, Scherwitzl R, Huang Y, Strocov V N, Zubko P, Balandeh S, Triscone J M, Sawatzky G and Schmitt T 2016 *Nat. Commun.* **7** 13017

[12] Mazin I I, Khomskii D I, Lengsdorf R, Alonso J A, Marshall W G, Ibberson R M, Podlesnyak A, Martínez-Lope M J and Abd-Elmeguid M M 2007 *Phys. Rev. Lett.* **98** 176406

[13] Johnston S, Mukherjee A, Elfimov I, Berciu M and Sawatzky G A 2014 *Phys. Rev. Lett.* **112** 106404

[14] Park H, Millis A J and Marianetti C A 2012 *Phys. Rev. Lett.* **109** 156402

[15] Garcia-Munoz J L, Rodriguez-Carvajal J and Lacorre P 1994 *Phys. Rev. B* **50** 978

[16] Rodríguez-Carvajal J, Rosenkranz S, Medarde M, Lacorre P, Fernandez-Díaz M, Fauth F and Trounov V 1998 *Phys. Rev. B* **57** 456

[17] Chen H, Kumah D P, Disa A S, Walker F J, Ahn C H and Ismail-Beigi S 2013 *Phys. Rev. Lett.* **110** 186402

[18] Torriss B, Margot J and Chaker M 2017 *Sci. Rep.* **7** 40915

[19] Bruno F Y, Rushchanskii K Z, Valencia S, Dumont Y, Carrétéro C, Jacquet E, Abrudan R, Blügel S, Ležaić M, Bibes M and Barthélémy A 2013 *Phys. Rev. B* **88** 195108

[20] Jin K J, Lu H B, Zhou Q L, Zhao K, Cheng B L, Chen Z H, Zhou Y L and Yang G Z 2005 *Phys. Rev. B* **71** 184428

[21] Jiang L T, Jin K J, Ma C, Ge C, Yang G Z and He X 2018 *Phys. Rev. B* **97** 195132

[22] Xu Z T, Jin K J, Gu L, Jin Y L, Ge C, Wang C, Guo H Z, Lu H B, Zhao R Q and Yang G Z 2012 *Small* **8** 1279

[23] Mikheev E, Hauser A J, Himmetoglu B, Moreno N E, Janotti A, Van de Walle C G and Stemmer S 2015 *Sci. Adv.* **1** e1500797

[24] He Z and Millis A J 2015 *Phys. Rev. B* **91** 195138

[25] Zhang J Y, Kim H, Mikheev E, Hauser A J and Stemmer S 2016 *Sci. Rep.* **6** 23652

[26] Varignon J, Grisolia M N, Íñiguez J, Barthélémy A and Bibes M 2017 *npj Quantum Materials* **2** 1

[27] Perdew J P, Ruzsinszky A, Csonka G I, Vydrov O A, Scuseria G E, Constantin L A, Zhou X and Burke K 2008 *Phys. Rev. Lett.* **100** 136406

[28] Kresse G and Furthmüller J 1996 *Phys. Rev. B* **54** 11169

[29] Kresse G and Joubert D 1999 *Phys. Rev. B* **59** 1758

[30] Dudarev S, Botton G, Savrasov S, Humphreys C and Sutton A 1998 *Phys. Rev. B* **57** 1505

[31] Mercy A, Bieder J, Iniguez J and Ghosez P 2017 *Nat. Commun.* **8** 1677

[32] Hampel A and Ederer C 2017 *Phys. Rev. B* **96** 165130

[33] Yoo P and Liao P 2020 *Phys. Chem. Chem. Phys.* **22** 6888

[34] Momma K and Izumi F 2011 *J. Appl. Crystallography* **44** 1272

[35] Kanamori J 1960 *J. Appl. Phys.* **31** S14

[36] Van V J H 1939 *J. Chem. Phys.* **7** 72